Supplementary Information for

A theoretical trend of oxygen vacancy levels in typical metal oxides

Zihui Chen,[1] Kan-Hao Xue,[1,*] Heng Yu,[1] Zijian Zhou,[1] Shanzhong Xie,[1] Xiangshui Miao[1]

[1]School of Integrated Circuits, Huazhong University of Science and Technology, Wuhan 430074, China

[*]Corresponding author, email: xkh@hust.edu.cn

Note 1. Computational settings

All calculations were performed using first-principles density functional theory (DFT) implemented in the Vienna ab initio simulation package (VASP). The self-energy corrected shell GGA-1/2 method was employed to calculate the density of states (DOS) of the supercell, using the PBEsol functional for exchange-correlation treatment. Projector augmented-wave (PAW) potentials (valence electrons were Hf: $5p^6 5d^3 6s^1$, Zr: $4s^2 4p^6 4d^3 5s^1$, Ti: $3s^2 3p^6 3d^3 4s^1$, Al: $3s^2 3p^1$, Ga: $3d^{10} 4s^2 4p^1$, O: $2s^2 2p^4$) were adopted. Supercell models were constructed as follows: HfO_2 in a 2×2×2 monoclinic phase ($P2_1/c$), ZrO_2 in a 2×2×2 monoclinic phase ($P2_1/c$), TiO_2 in a 3×3×4 rutile phase ($P4_2/mnm$), Al_2O_3 in a 2×2×1 α-phase ($R\bar{3}c$), and Ga_2O_3 in a 1×4×2 β-phase ($C2/m$), with atomic positions fully relaxed until residual forces fell below 0.02 eV/Å. A consistent plane-wave kinetic cutoff energy of 500 eV and 4×4×4 Monkhorst-Pack k-mesh were applied across all these supercells.

Note 2. Computational details and results for TiO_2

Since shell GGA-1/2 tends to over-estimate the Vo-level, this risks pushing the Vo defect states into the conduction band for TiO_2. Hence, we further adopted an on-site Hubbard U correction for the Ti 3d orbitals, with $U - J =$ 4.2 eV. The as-derived partial density of states results and electronic band structures are illustrated in **Figure S1**.

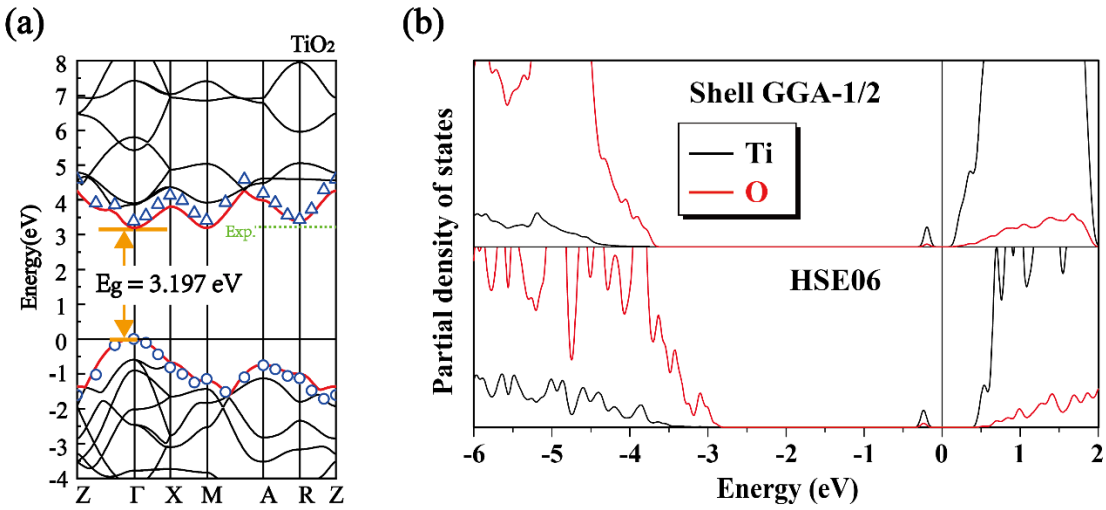

Figure S1. (a) Electronic band diagrams of rutile TiO_2, calculated using shell GGA-1/2 (continuous curves) and HSE06 (discrete points). The VBM is set to zero energy; (b) Partial density of states analyses to a defective TiO_2 supercell with Vo.

Note 3. Supercell size convergence and speed testing

While shell GGA-1/2 and HSE06 demonstrate similar qualities in terms of the band structure, the time saving of shell GGA-1/2 is considerable. To ensure a fair comparison, we conducted comparative self-consistent band structure calculations on rutile TiO_2, by specifying explicitly 24 irreducible k points and 24 zero-weight k points. With the same 64-core computer, shell GGA-1/2 finishes in 9.81 s while HSE06 costs 9814.38 s. The computational load of HSE06 is typically 3 orders of magnitude higher than shell GGA-1/2. The efficient nature of shell GGA-1/2 thus enables defective supercell calculations with very large cell sizes.

The subsequent issue lies in how large a supercell is adequate to extract the defect-induced trap levels. This requires setting up various sizes of the supercell to examine any discrepancy in trap levels. To be specific, we introduced one oxygen vacancy in $2 \times 2 \times 2$, $3 \times 3 \times 3$ and $4 \times 4 \times 4$ monoclinic HfO_2 supercells, whose initial atom numbers per cell are 96, 324 and 768, respectively. After optimizing the atomic coordinates within each supercell using GGA, shell GGA-1/2 calculations were performed to yield the density of states (DOS). The as-derived DOS results are illustrated in **Figure S2** without normalization. In other words, the $4 \times 4 \times 4$ supercell will exhibit the strongest DOS values. Yet, the benefit lies in that the defect-induced states can be compared at the same footing, and they tend to overlap whenever the defect states are independent of the supercell size as far as these three enlarged cells are concerned. In **Figure S2**, one cannot even discriminate the defect DOS from the three calculations, while the conduction band and valence band DOS values show the consistent enhancement upon increasing the supercell size. When it comes to the defect formation energy, various supercell sizes do lead to slight differences, as observed in **Table S1**. Nevertheless, compared with the Vo formation energy, the electronic structure is much less sensitive to the supercell size in HfO_2, thus a $2 \times 2 \times 2$ supercell is sufficient for a single oxygen vacancy-related studies. The other three materials exhibit the same trend.

Table S1. Vo-formation energies calculated using various supercells and the PBEsol functional.

Material	Supercell	Vo formation energy (eV)
HfO_2	2 × 2 × 2	7.323
	3 × 3 × 3	7.373
	4 × 4 × 4	7.370
TiO_2	2 × 2 × 4	6.550
	3 × 3 × 4	6.541
	4 × 4 × 5	6.544
Al_2O_3	2 × 2 × 1	7.645
	3 × 3 × 1	7.698
	4 × 4 × 1	7.695
Ga_2O_3	1 × 4 × 2	4.628
	1 × 5 × 3	4.733
	2 × 6 × 3	4.699

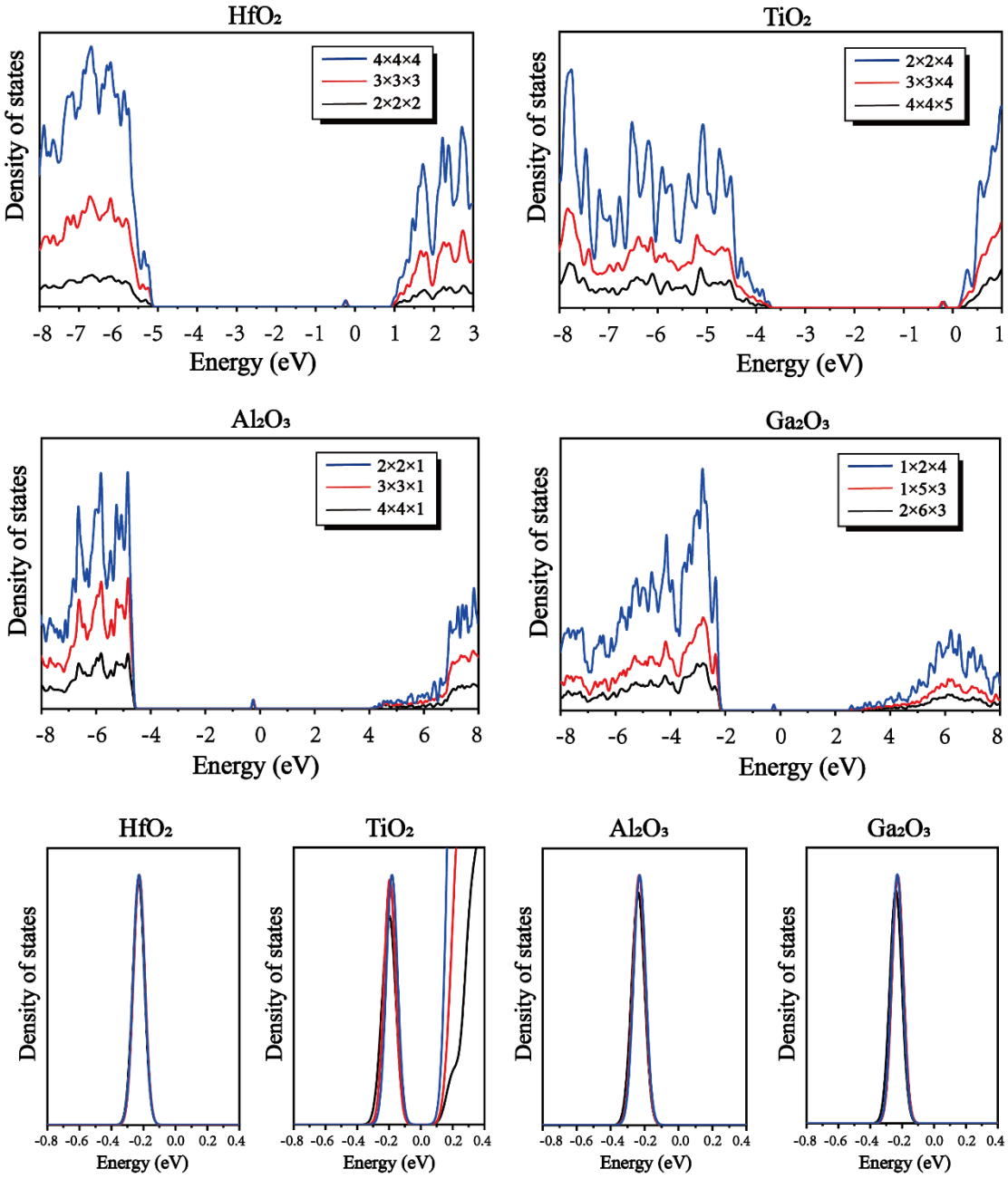

Figure S2. Electronic density of states for the four defective oxides, calculated using various sizes of supercells with one oxygen vacancy per cell. All calculations used shell GGA-1/2.

Note 4. Charge transition level calculation

An accurate charge transition level (CTL) calculation requires both total energy accuracy and precise electronic band structure, including the band gap. DFT-1/2 and shell DFT-1/2 rectify the band gap, but their total energies cannot be used since the considered state is a "transition state" due to Slater. Such a state is apparently treated as a "ground state" in the self-consistent calculation cycle, but it is physically linked to the transition state during excitation, such that the as-derived electronic structure results can recover the quasi-particle structure. While this favors reasonable band gaps, the total energy is no longer the ground state energy. GGA calculations yield reasonable total energy differences for these oxides under consideration, but the band gap is over-low. Hence, we refer to HSE06 hybrid functional calculations for CTL derivation. While sufficiently dense k-meshes were adopted for primitive cell relaxation, a consistent $2 \times 2 \times 2$ k-mesh was used for any supercell structural optimization and total energy calculation in terms of HSE06. All structural relaxations using the HSE06 functional were carried out with spin polarization, and the plane wave kinetic energy cutoff was fixed to 500 eV. For comparative reasons, CTL calculations using GGA were still carried out.

The formation energy of a possibly charged oxygen vacancy defect is given by

$$E_f^{q+} = E_{\mathrm{d}}^{q+} - E_0 + \mu_{\mathrm{O}} + q(E_v + E_F + \Delta V)$$

where E_{d}^{q+} is the total energy of the +q charged defective supercell after relaxation, E_0 is the total energy of the perfect oxide in the same supercell size, μ_{O} is the chemical potential of oxygen that is regarded as half the total energy of an isolated O_2 molecule, E_v is the VBM position and E_F is the system's Fermi level with respect to VBM. And ΔV is the electron average potential energy shift in the charged supercell, with respect to the perfect supercell. It is taken from the electrostatic potential energy difference (unit: eV) between the charged defective supercell and the perfect supercell, counted from a cation distinct from the Vo site as well as an anion distinct from the Vo site.

$$\Delta V_{\mathrm{cation}} = V_{\mathrm{cation}}^{\mathrm{defective}} - V_{\mathrm{cation}}^{\mathrm{perfect}}$$

$$\Delta V_{\mathrm{anion}} = V_{\mathrm{anion}}^{\mathrm{defective}} - V_{\mathrm{anion}}^{\mathrm{perfect}}$$

The potential shift is simply their mathematical average

$$\Delta V = \frac{\Delta V_{\text{cation}} + \Delta V_{\text{anion}}}{2}$$

For a neutral Vo, its formation energy is simply, by setting $q = 0$,

$$E_f^{Neutral} = E_d - E_0 + \mu_{\text{O}}$$

To calculate the CTL, one requires that

$$E_f^{q+} = E_f^{Neutral}$$

such that

$$E_F = E_{\text{F}}^{critical} = \frac{E_d - E_{\text{d}}^{q+}}{q} - E_v - \Delta V$$

is the condition for this balance. Hence,

$$\text{CBM} - \text{CTL} = E_g - E_{\text{F}}^{critical} = E_v + E_g + \Delta V + \frac{E_{\text{d}}^{q+} - E_d}{q}$$

The choice of μ_{O} does not impact the CTL level at all, therefore we simply take the value from GGA calculations.

The CTL calculation results are given in **Table S2**. For each material, the selected supercell contains at least 96 atoms. To ensure that the size is sufficiently large for a charged cell calculation, we examined the size-effect using GGA. On the one hand, HSE06 becomes too heavy for a supercell of over 500 atoms. On the other hand, the central part of the image charge effect lies in the E_{d}^{2+} term, and it becomes necessary to investigate whether the 96-atom supercell is large enough after ΔV correction. We took V_{O3} in monoclinic HfO_2 as the benchmark. **Table S3** shows that, upon enlarging the $2 \times 2 \times 2$ supercell to $3 \times 3 \times 3$ and $4 \times 4 \times 4$, the variation of CTL is at the 0.01 eV level. This implies that a 96-atom supercell is adequate to extract CTL for monoclinic HfO_2.

Table S2. The charge transition level results through HSE06 calculations.

Material and Vo site	HfO_2		ZrO_2		TiO_2	Al_2O_3	Ga_2O_3
	V_{O3}	V_{O4}	V_{O3}	V_{O4}			
Atoms per supercell	96		96		96	120	120
Energy from HSE06 calculation (eV)							
$E_d - E_0$	13.652	13.561	13.388	13.313	7.813	14.263	11.358

$E_{\mathrm{d}}^{2+}-E_0$	1.289	2.068	-4.479	-3.650	-2.049	-3.400	1.353
ΔV	0.070	0.049	0.043	0.039	-0.113	0.144	0.100
μ_{O}	-4.442						
VBM（E_v）	2.178	2.178	4.898	4.898	3.919	4.767	2.473
E_g	5.662	5.662	5.286	5.286	3.442	7.992	4.159
CBM−CTL	1.729	2.143	1.293	1.742	0.096	4.071	1.729
Exp. CBM-CTL	1.5 [1]	2 [1]	1.16 [2]	/	/	/	/
Comparative result from shell DFT-1/2 calculation (eV)							
E_1	0.947	1.434	0.479	0.765	0.194	4.217	2.510

Table S3. The impact of supercell size on the CTL result of V_{O3} in monoclinic HfO_2, using GGA.

Supercell	Atom count	Energy (eV)		
		ΔV	CTL-VBM	CBM-CTL*
$2\times2\times2$	96	0.058	2.856	1.105
$3\times3\times3$	324	0.049	2.859	1.102
$4\times4\times4$	768	0.046	2.835	1.126

*These values are problematic due to the severe band gap underestimation by GGA.

Note 5. Details of the doped model supercells

To investigate the dopant-induced modulation of oxygen vacancy (Vo) defect states in doped systems, we constructed defect-containing supercells by selectively substituting metal atoms adjacent to the targeted oxygen vacancy with dopant atoms**.** This site-specific substitutional doping strategy prioritizes nearest-neighbor positions, where the defect formation energy of the oxygen vacancy is minimized, which thermodynamically favors oxygen vacancy stabilization. Taking Al-doped β-Ga_2O_3 as an example, as illustrated in **Figure S3**. The oxygen vacancy exhibits bond lengths of 1.842 Å, 1.942 Å, and 3.616 Å to adjacent Ga atoms. We substituted the Ga atom at 1.842 Å with respect to the Vo, by Al, to maximize dopant-vacancy proximity. The same processing method is used for other materials.

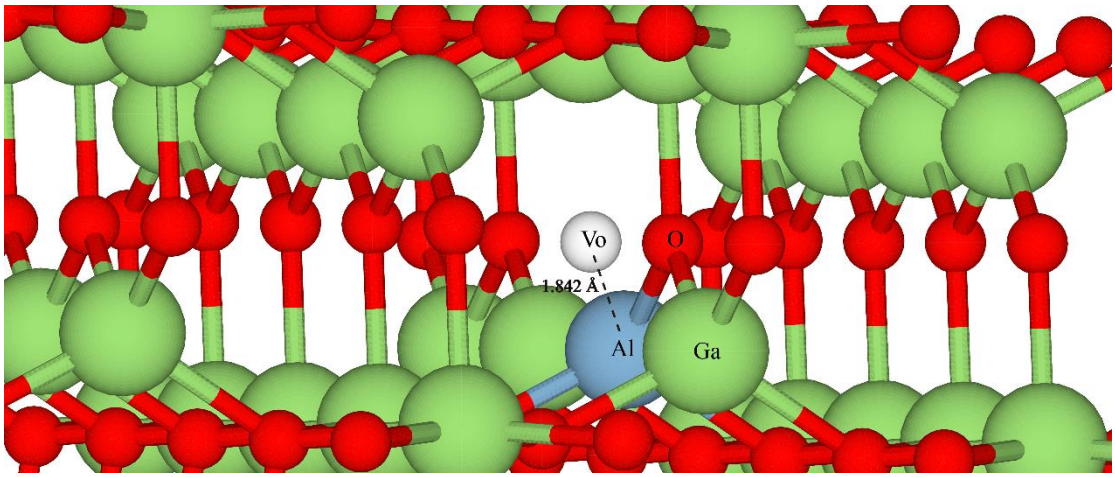

Figure S3. Schematic view of the defective model supercell with a dopant (Al-doped β-Ga_2O_3).

Note 6. Formation energy of the Al vacancy in Al_2O_3 and the Ga vacancy in Ga_2O_3

We calculated the energy of Al_2O_3 without defects, Al_2O_3 with oxygen vacancy defects, Ga_2O_3 without defects, and Ga_2O_3 with oxygen vacancy defects, separately. According to the formula for neutral defect formation energy calculation,

$$E_f = E_d - E_0 + \mu_M$$

where μ_M is the chemical potential of the metal element. We took μ_M as the total energy per atom in the corresponding bulk metal, *i.e.*, Al in face-centered cubic phase and Ga in the orthorhombic phase. We calculated the cation vacancy formation energies ($E_f[V_{cat}]$) for V_{Al} in Al_2O_3 and V_{Ga} in Ga_2O_3, as reported in the main text. The computational methodology and results are shown in **Table S4**.

Table S4. Computational details for the metal vacancy formation.

Material	α-Al_2O_3	β-Ga_2O_3
Supercell	120-atom (2 × 2 × 1 expansion)	160-atom (1 × 4 × 2 expansion)
XC	GGA-PBEsol	GGA-PBEsol
Plane wave cutoff energy	500 eV	500 eV
k-point mesh	Monkhorst-Pack 4 × 4 × 4	Monkhorst-Pack 4 × 4 × 4
Force convergence	0.02 eV/Å	0.02 eV/Å
Formation energy $E_f[V_{cat}]$	12.598 eV	9.957 eV

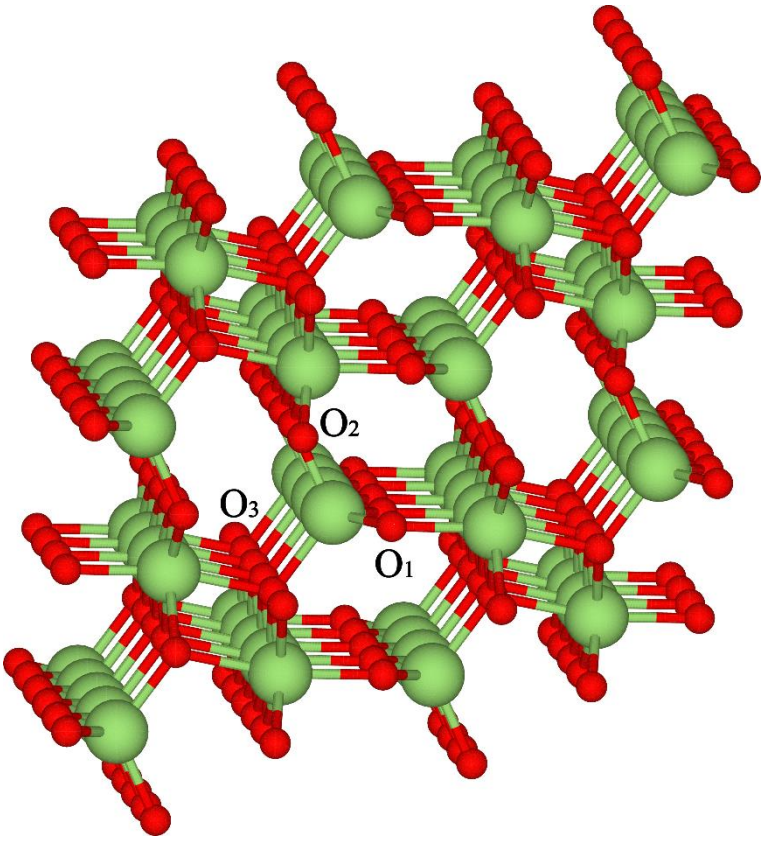

Figure S4. Illustration of the three distinct O sites in β-Ga_2O_3. Both O1 and O2 are in three-coordination, while O3 is in four-coordination.

Note 7. Formation energy as a function of atom-atom distance in the structural relaxation

Since only neutral oxygen vacancies are involved in our Kohn-Sham defect level approach (not the CTL approach), we adopted the energy-minimized structure obtained from structural relaxation as the ground state. To preclude the possibility of other metastable configurations, we computed the energies of a series of intermediate configurations by relaxing all degrees of freedom except the interatomic distance. The results confirm that the structures we employed correspond to the global energy minima, with no other local energy minima observed. We selected the material exhibiting the most pronounced structural distortion before and after relaxation—α-Al_2O_3 doped with Ga—as an illustrative example to describe this procedure. In α-Al_2O_3, an oxygen atom forms a short bond (SB) of 1.861 Å and a long bond (LB) of 1.974 Å with neighboring Al atoms. A neutral oxygen vacancy was created by removing this oxygen atom, and the Al atom on the long-bond side was substituted by a Ga atom. We denote this Ga atom as Ga(0) and the Al atom on the short-bond side as Al(0). Structural relaxation reveals that Al(0) remains largely undistorted, whereas Ga(0) undergoes significant displacement. We fixed eleven different Ga(0)–Al(0) distances and performed full structural relaxation for each configuration. **Figure S5** shows the formation energy during relaxation as a function of the Ga(0)–Al(0) distance. It is evident that the energy monotonically decreases as the distance shortens, with no additional energy minima present, thereby precluding the existence of metastable states.

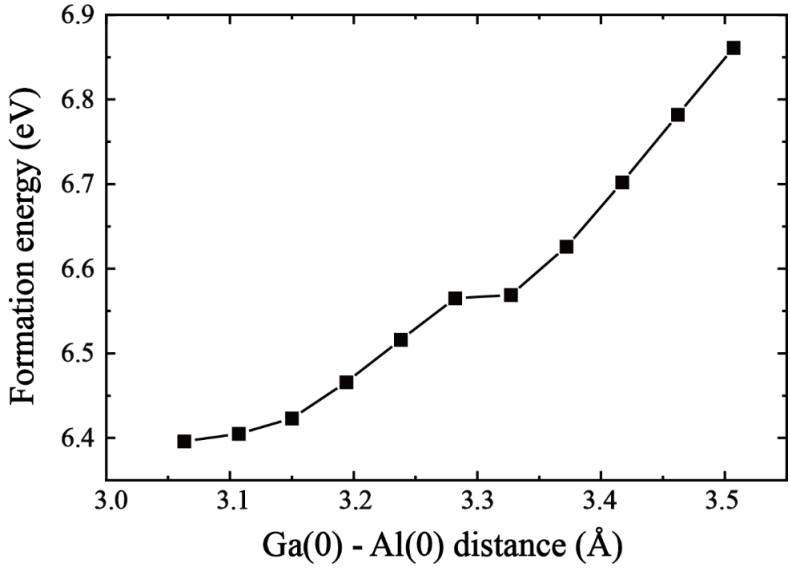

Figure S5. Formation energy as a function of Ga(0)-Al(0) distance in Ga-doped Al_2O_3.

Additional supplementary data

The calculated density of states (DOS) reveals the formation of a prominent trap level within the forbidden band due to the oxygen vacancy (**Figure S6**). This in-gap trap state, which is absent in the vacancy-free system, can effectively capture charge carriers and serve as a recombination center, thereby critically influencing the electronic properties of the material.

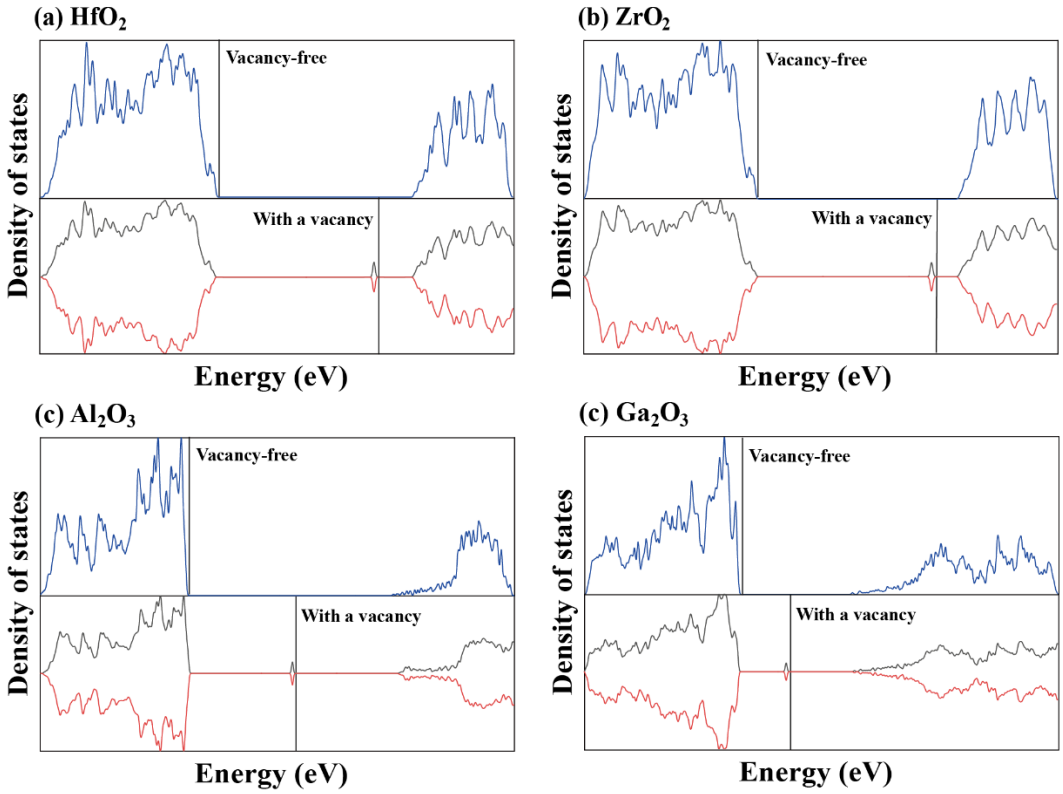

Figure S6. Density of states analyses to vacancy free system and defective system with a vacancy.

Table S5. HSE06 calculation supplementary data.

Material	Supercell	Method	E_g (eV)	E_1 (eV)	E_2 (eV)	γ
HfO_2 $V_{O\text{-}III}$	2 × 2 × 2	HSE06	5.100	1.915	3.185	1.66 > 1
HfO_2 $V_{O\text{-}IV}$	2 × 2 × 2	HSE06	4.972	2.424	2.548	1.05 > 1
ZrO_2 $V_{O\text{-}III}$	2 × 2 × 2	HSE06	4.664	1.401	3.263	2.33 > 1
ZrO_2 $V_{O\text{-}IV}$	2 × 2 × 2	HSE06	4.591	1.886	2.705	1.43 > 1
TiO_2	3 × 3 × 4	HSE06	2.782	0.413	2.369	5.74 > 1
Al_2O_3	2 × 2 × 1	HSE06	7.597	4.890	2.707	0.55 < 1
Ga_2O_3 V_{O1}	1 × 4 × 2	HSE06	3.683	2.811	0.872	0.31 < 1

References

[1] Kruchinin V N, Aliev V Sh, Perevalov T V, et al. Nanoscale potential fluctuation in non-stoichiometric HfO_x and low resistive transport in RRAM. *Microelectronic Engineering* **147**, 165 (2015).

[2] Kumar A, Mondal S, Rao K S R K. Experimental evidences of charge transition levels in ZrO_2 and at the Si:ZrO_2 interface by deep level transient spectroscopy. *Applied Physics Letters* **110**, 132904 (2017).